Microstructures and mineral chemistry in amphibolites from the western Tauern Window (Eastern Alps), and $P-T$ deformation paths of the Alpine greenschist-amphibolite facies metamorphism

BERNHARD SCHULZ

Institut für Geologie und Mineralogie der Universität, Schloßgarten 5, D-91054 Erlangen, Germany

CLAUDE TRIBOULET

Laboratoire de Pétrologie Minéralogique, C.N.R.S. U.R.A. 736, Université Pierre et Marie Curie, 4 place Jussieu, F-75252 Paris Cedex 05, France

AND

CLAUDE AUDREN

Géosciences Rennes, Laboratoire Tectonophysique, Institut de Géologie, Avenue du Général Leclerc, F-35042 Rennes Cedex, France

Abstract

Amphibolites in the Mesozoic part of the parautochthonous Lower Schieferhülle (LSH), the allochthonous Upper Schieferhülle (USH) and the overlying Austroalpine basement (AA) in and around the western Tauern Window (Eastern Alps) suffered a progressive Alpine deformation. Lineations and foliations L_1-S_1, L_2-S_2 defined by preferentially oriented (Na-Ca) amphiboles as well as F_3 folds and further foliations S_{myl} and S_4 in the metabasites are structures of successive deformational stages with a constant W–E main extension axis of strain. The (Na-Ca) amphiboles in assemblages with epidote, chlorite, albite/oligoclase and quartz are zoned with similar continuous zonation trends from early actinolite in the cores to magnesio-hornblende and tschermakitic hornblende, and from magnesio-hornblende to late actinolite in the rims in the three lithostratigraphic units. Geothermobarometry involving tremolite-edenite and (pargasite–hastingsite)–tremolite end-member equilibria in amphiboles allowed us to reconstruct prograde–retrograde $P-T$ paths for the Alpine greenschist-amphibolite facies event. The paths passed P/T_{max} at 6–7 kbar/600°C. Similar shapes of the paths in AA, USH and Mesozoic LSH indicate a common metamorphic history and a stacking of these units prior to or during the pre-P_{max} evolution. Moderate $P-T$ ratios are characteristic for the temperature-dominated compression paths and indicate continental collisional rather than subduction zone metamorphism. The middle to late Alpine greenschist–amphibolite facies event appears as an independent metamorphism along a complete $P-T$ loop which may have followed an earlier and poorly documented high-pressure/low-temperature event.

KEYWORDS: amphibolites, microstructures, geothermobarometry, $P-T-t$-deformation paths, Alpine orogeny, western Tauern Window.

Mineralogical Magazine, December 1995, Vol. 59, pp. 641–659

Introduction

MINERAL equilibria and various methods of geothermobarometry have been successfully applied to reveal the pressure-temperature ($P-T$) evolution of the Alpine metamorphism in and around the Tauern Window. Early studies focused mainly on the quantification of maximal pressures and temperatures of successive stages of metamorphism. However, even if precise, such data only poorly describe the thermobarometric evolution of a metamorphic terrain. For a profound geological interpretation in terms of a comparison with numerical tectonothermal $P-T$ models, it is necessary to reconstruct prograde and/or retrograde $P-T$ paths as complete as possible from single samples or locations (Spear, 1993). The relationship between the geothermobarometric, the temporal (t) and the structural evolution of the rocks, the $P-T-t$-deformation (d) path improves this knowledge further.

Assemblages with growth zoned garnets in metapelites have recorded a history of continuous reaction and $P-T$ changes during metamorphism. This has been used by Spear and Selverstone, (1983), Selverstone *et al.*, (1984), Selverstone and Spear, (1985), von Blanckenburg *et al.*, (1989), Selverstone, (1993), Christensen *et al.*, (1994) to reconstruct $P-T-t$ paths from the western Tauern Window.

Chemical zonations of (Na-Ca) amphiboles in equilibrium with epidote, chlorite, albite and quartz in metabasites provide an alternative way to determine continuous variations of $P-T$ conditions

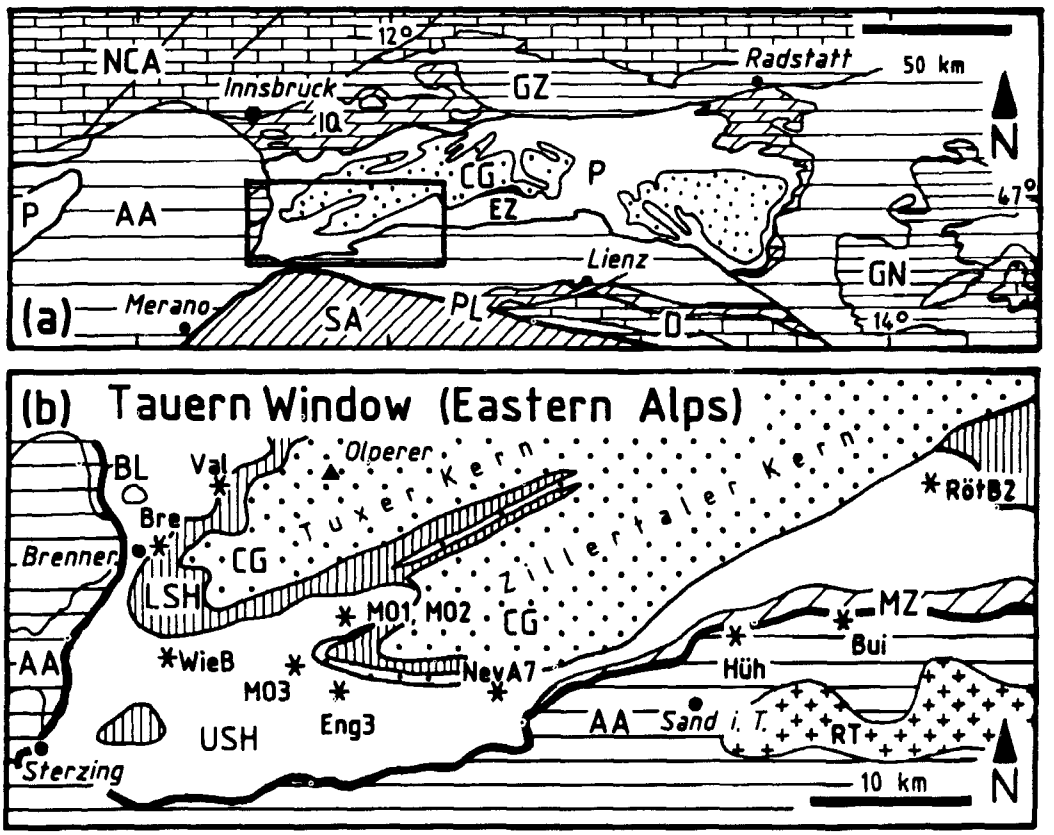

FIG. 1. (*a*) Geological setting in the Eastern Alps. (*b*) Lithostratigraphic units in the western Tauern Window and its frame, and sample locations. AA—Austroalpine basement; BL—Brenner Line; CG—Central gneisses; D—Mesozoic of Drauzug; EZ—Eclogite zone; GN—Gurktal nappes; GZ—Grauwackenzone; IQ—Innsbrucker Quarzphyllit; LSH—Lower Schieferhülle; MZ—Matreier zone; NCA—Northern Calcareous Alps; P—Penninic unit; PL—Periadriatic Line; RT—Rieserferner tonalite (Oligocene); SA—Southern Alps; USH—Upper Schieferhülle.

(e.g. Holland and Richardson, 1979; Triboulet and Audren, 1988; Triboulet, 1992). The present study describes zoned (Na-Ca) amphiboles and related microstructures in metabasites from the Penninic western Tauern Window and the overlying Austroalpine nappe. Complete prograde–retrograde $P-T$ paths from these rocks are directly correlated to the L-S structures of a polyphase Alpine deformation. This led to precise knowledge about the Alpine tectonothermal evolution in the Eastern Alps.

Regional metamorphic and structural setting

The Tauern Window is an erosional window in which the metamorphic rocks of the Penninic zone are exposed below the Austroalpine units (Fig. 1). Several main tectonostratigraphic units can be distinguished: The structurally lowest units are the Zentralgneis (CG), a pre-Variscan basement complex ('Altkristallin', 'old roof') intruded by late-Variscan granitoids overlain by a post-Variscan Permian to Lower Cretaceous cover sequence. Both pre-Variscan and post-Variscan sequences occur in a parautochthonous position and together comprise the Lower Schieferhülle (LSH). These units with Helvetic affinity (Lammerer, 1988) are overthrusted by the Upper Schieferhülle (USH), which is a Penninic ophiolite nappe ('Glockner nappe') of Jurassic to early Cretaceous rocks. (Höck, 1969; Thiele, 1970; Morteani, 1971; 1974; Tollmann, 1977; Raith *et al.*, 1977; 1980; De Vecchi and Baggio, 1982; De Vecchi and Mezzacasa, 1986; Lammerer, 1986; Frank *et al.*, 1987). Between Lower and Upper Schieferhülle in the central part of the Tauern Window is the Eclogite zone (EZ), a slice of high-pressure metabasites, metacarbonates and metapelites. The southern margin of the Upper Schieferhülle is marked by a varied sequence of Mesozoic rocks, called the Matreier zone (MZ). Biotite-gneisses, mylonitic orthogneisses, amphibolites and a sequence of garnet muscovite schists are found in the lowermost parts of the overlying pre-Variscan basement ('Altkristallin') of the Austroalpine crystalline nappe (AA) (Senarclens-Grancy, 1972; Hofmann *et al.*, 1983; Schulz, 1994).

The western and central parts of the Tauern Window are sites of classical as well as modern studies on Alpine metamorphism and $P-T-t-d$ paths. A first and presumably early-Alpine high-pressure event at 550–600°C/18–20 kbar is documented by rocks of the Eclogite zone (Miller, 1977; Miller *et al.*, 1980; Holland, 1979; Spear and Franz, 1986; Frank *et al.*, 1987) which show Eocene (36 Ma) Ar-Ar cooling ages (Zimmermann *et al.*, 1994). Relics of a second metamorphic event around 450°C/> 7–9 kbar at 90–60 Ma (Holland and Richardson, 1979; Raith *et al.*, 1978; 1980) or younger as Upper Eocene (Zimmermann *et al.*, (1994), referred to as the blueschist or glaucophane-lawsonite event, occur in some metabasites of the Eclogite zone. Holland and Ray (1985) described crossite and jadeitic pyroxene from metabasites of the USH. Furthermore, lozenge-shaped mineral aggregates in metabasites of the USH have been interpreted as pseudomorphs after lawsonite (Fry, 1973; Holland, 1979; Höck, 1980; Selverstone and Spear, 1985; Frank *et al.*, 1987*a*; Dachs *et al.*, 1991). Both observations signalize a blueschist event outside the Eclogite zone.

A younger greenschist-amphibolite facies event, the 'Tauernkristallisation' of Sander (1912; 1921), affected all tectonostratigraphic units and rock types in the western and central Tauern Window. Maximal pressures of 6–7 kbar and maximal temperatures near 550°C were reported from the USH and contrast higher pressures of 10 kbar and temperatures up to 600°C in the LSH (e.g. Hoernes and Friedrichsen, 1974; Höck, 1980; Höck and Hoschek, 1980; De Vecchi and Baggio, 1982; Dachs, 1990). The $P-T$-time evolution of this metamorphism has been investigated by Spear and Selverstone (1983), Selverstone *et al.* (1984), Selverstone and Spear (1985), Selverstone (1988; 1993), von Blanckenburg *et al.* (1989), Lammerer and Morteani (1990) and Christensen *et al.* (1994). Ages by Rb-Sr of between 60 and 30 Ma, from garnets, were interpreted to show that crystallization occurred at around P_{max} (Selverstone, 1993). Raith *et al.* (1978) reported K-Ar ages of 42.5 Ma from actinolite cores and of 24 Ma from green hornblende rims in zoned amphiboles from the USH in the Ahrntal (Italy). The range of phengite Rb-Sr, hornblende K-Ar, phengite K-Ar, biotite-Rb-Sr, K-Ar and apatite FT ages continuously decreased from 20 to 7 Ma during subsequent cooling/uplift (Grundmann and Morteani, 1985; von Blanckenburg *et al.*, 1989). Few data exist on the Alpine metamorphism of the overlying Austroalpine basement (AA) to the south of the Tauern Window. Conditions of 400–450°C/7 kbar (Stöckhert, 1984) of an early stage of Alpine metamorphism, with maximum temperatures of approx. 550°C (Schulz, 1990), and a late-Alpine stage at 350°C/3–4 kbar (Stöckhert, 1984; Kleinschrodt, 1987) have been reported. A phengite K-Ar age of 100 Ma (Stöckhert, 1984) on one side and biotite Rb-Sr ages from 28 to 15 Ma (continuously younger toward the southern rim of the Tauern Window: Borsi *et al.*, 1978; Hammerschmidt, 1981) on the other side, indicate a polyphase Alpine history or a mixing of pre-Alpine and Alpine ages.

Prominent Alpine deformational structures such as foliation, lineation and fold axes are concordant in the LSH, USH and AA units (Nollau, 1969; Kleinschrodt, 1987; Lammerer *et al.*, 1981). Recent

tectonic models for the Alpine evolution in the Tauern Window describe an early thrust regime followed by a transpressional regime (Lammerer, 1988; Oehlke *et al.*, 1993). Stacking of the tectonostratigraphic units is related to a deformation D_1. Structural features of this event and clues for the transport direction were erased by the subsequent deformation. A main foliation S_2 of oblate ductile shearing D_2 is penetrative in metasediments, metabasites and gneisses, and axial-planar to isoclinal folds F_2. The D_2 structures were overprinted by prolate deformation D_3 with tight folding. The W–E trending F_3 fold axes together with parallel mineral lineations may indicate dextral transpressional movements during D_3 (Lammerer, 1988; Schön and Lammerer, 1993; Oehlke *et al.*, 1993). Selverstone (1988) related the retrograde evolution of the greenschist-amphibolite facies event to a W–E directed extensional ductile thinning, then top-to-W directed low-angle normal faulting.

In view of the wealth of petrological, structural, radiometric and geochemical data, the western and central Tauern Window serves as an apparently well known example for tectonothermal models of

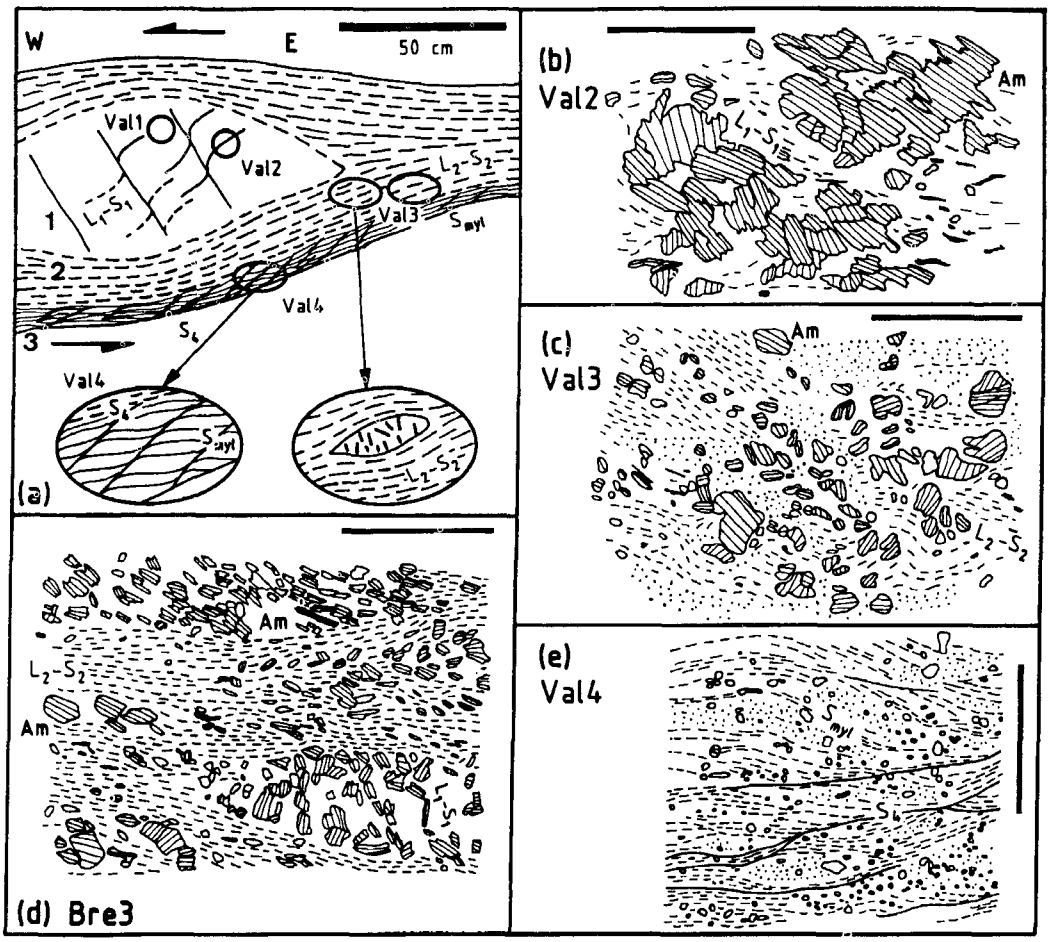

FIG. 2. (*a*) Mesoscopic structures and sampling points in an amphibolite of the Lower Schieferhülle at the location Valser Tal. L_1-S_1, L_2-S_2, S_{myl}, S_4 are linear and planar structures. Shear sense criteria indicates top-to-W transport. 1, 2, 3 are structural domains (see text). (*b*) Large amphiboles in dm-scale structural domain 1. (*c*) Amphiboles and L_2-S_2 in foliated domain 2. (*d*) L_2-S_2 structures and microlithon with large amphiboles of domain 1 in a foliated domain 2 at the Brenner location. (*e*) Epidote chlorite schist of domain 3 with mylonitic foliation S_{myl} and shearband foliation S_4. Scale bar in (*b*)–(*e*) is 1 cm.

orogenic processes and the related metamorphism, especially subduction and continental collision (e.g. Frisch, 1976; Selverstone, 1988; Behrmann, 1990; Spear, 1993). However, several important aspects of the Alpine metamorphic evolution in the western Tauern Window remain weakly constrained. There exists only poor knowledge of the prograde metamorphism, and apart from the $P-T$ path studies (Selverstone *et al.*, 1984; Selverstone and Spear, 1985) there is little information about the spatial $P-T$ evolution within the tectonostratigraphic pile, especially from the Austroalpine unit. Amphibolites with different provenance and protolith ages but similar mineral assemblages and mineral chemistry occur in the Mesozoic part of the LSH, the USH and in the AA units. These rocks are suitable for a comparative study of the Alpine thermobarometric evolution of these units (Fig. 1*b*).

Microstructures and mineral chemistry in amphibolites

Lower Schieferhülle (LSH). A 1–3 m thick amphibolite horizon, probably an original dolerite sill, has been sampled in the mainly clastic Lower Cretaceous Kaserer formation (Höck, 1969; Thiele, 1970; Frisch, 1980, 1984) at Brenner Pass (samples: Bre) and in the Valser Tal (samples: Val). The locations represent the upper Mesozoic part of the Lower Schieferhülle LSH (Fig. 1*b*). The amphibolite horizon is subdivided into different mesoscopic structural domains (Fig. 2*a*). Decimeter-scale lens-like domains (1) with randomly or poorly arranged large amphiboles up to 5 mm in length and a weak foliation S_1 (Fig. 2*b*) are surrounded by medium- to fine-grained and strongly foliated domains (2) (Fig. 2*a*). Preferentially oriented amphiboles in domain (1) define an E–W striking mineral lineation L_2 on the foliation planes S_2. Sometimes cm-scale lenses of domain (2) with large amphiboles occur between the S_2 planes (Fig. 2*a,d*). Domain (3) is a fine-grained and finely-banded foliated (S_{myl}) epidote chlorite schist at the base of the amphibolite horizon. A shearband foliation, S_4, cuts across the mylonitic foliation S_{myl} at an acute angle and with a top-to-W directed sense of shear parallel to the W–E stretching lineation (Fig. 2*a,e*).

Microstructures and mineral chemistry have been studied in XZ sections parallel to the W–E trending mineral and stretching lineations (= X) and perpendicular to the foliation planes (= XY) of finite strain. Large first generation amphiboles (1) of L_1-S_1 occur in domain (1) and in microlithons between the foliation planes in domain (2) (Fig. 3*a,b,f*). Tension cracks between fragments of amphibole (1) are filled by chlorite, calcite, albite, epidote and quartz (Fig. 3*a,b*). A second amphibole generation (2) in domain (2) is preferentially oriented with the long axes parallel to S_2 and L_2 (Fig. 3*a–e,g*). Chlorite, epidote, albite and quartz are fine-grained in S_2 and coarse-grained when associated with amphibole (1) porphyroblasts. Amphibole (1) in domain (1) are actinolitic hornblende, magnesio-hornblende and sometimes tschermakitic hornblende with small cores of actinolite (Fig. 3*b,f*). Some of these large amphiboles (1) have narrow rims of actinolitic hornblende and actinolite (Fig. 3*a*). The actinolitic rims surround the fragments of large broken amphiboles with tension cracks, but are lacking when the porphyroblasts are broken along S_2 planes (Fig. 3*a*). Similar chemical zonation trends occur in amphibole (2), elongated in the foliation S_2 of domain (2) (Fig. 3*a*). Circular or lenticular cores by actinolite are mantled by actinolitic hornblende and magnesio-hornblende of which long axes are oriented parallel to the foliation/lineation (Fig. 3*a,c,d*). Some of the amphiboles (2) were stretched and broken. Actinolitic rims crystallized with albite and chlorite in the tension cracks as well as in a pressure shadow position (Fig. 3*a,b*). Needle-like small amphiboles (2) parallel to S_2 are poorly zoned with actinolitic hornblende cores and actinolite in the rims (Fig. 3*a*).

The (Na-Ca)-amphiboles are continuously zoned with Si 7.85 to 6.45, Al^{VI} 0.08 to 1.065, $(Na + K)_A$ 0.01–0.45 and Ti 0.002–0.053 (always per formula unit p.f.u., the site allotment is explained below) from actinolite cores to tschermakitic hornblende rims. Zonations from magnesio-hornblende to actinolite rims are continuous as well (Fig. 3*a–d*, Table 1). Actinolitic hornblende with Si 7.45, Al^{VI} 0.4–0.5, $(Na + K)_A$ 0.08–0.2 and Ti 0.016–0.025 of a late stage of crystallization occur in sample Bre3 (Fig. 3*a*). Strongly plastically deformed lens-shaped amphiboles were rarely preserved between the mylonitic foliation in the epidote chlorite schist of domain (3) at the base of the amphibolite horizon. Green amphibole is not stable within the fine-grained epidote, chlorite, albite, actinolite and quartz of S_{myl}.

Oligoclase is lacking in samples Bre and Val2 and all plagioclase is albite. Most of the plagioclase in sample BreB1 and Bre3 is albite, but oligoclase (An20) as well as albite crystallized parallel to S_2 in domain (2) in equivalent microstructural positions. Only oligoclase has been found in sample BreA1. There appears to be no systematic variation of amphibole compositions with the occurrence of oligoclase or albite or both in the samples. The Fe-rich epidotes are poorly zoned with Al^{3+} between 2.5 and 2.6 in the studied samples. Chlorites in domains (1) and (2) are homogeneous with X_{Mg} 0.65–0.68 in the Bre samples and 0.56 in the Val samples.

From the microstructural and mineral chemistry observations it is concluded that the structural domains (1) and (2) both existed during the growth of early actinolite, then green hornblende and late

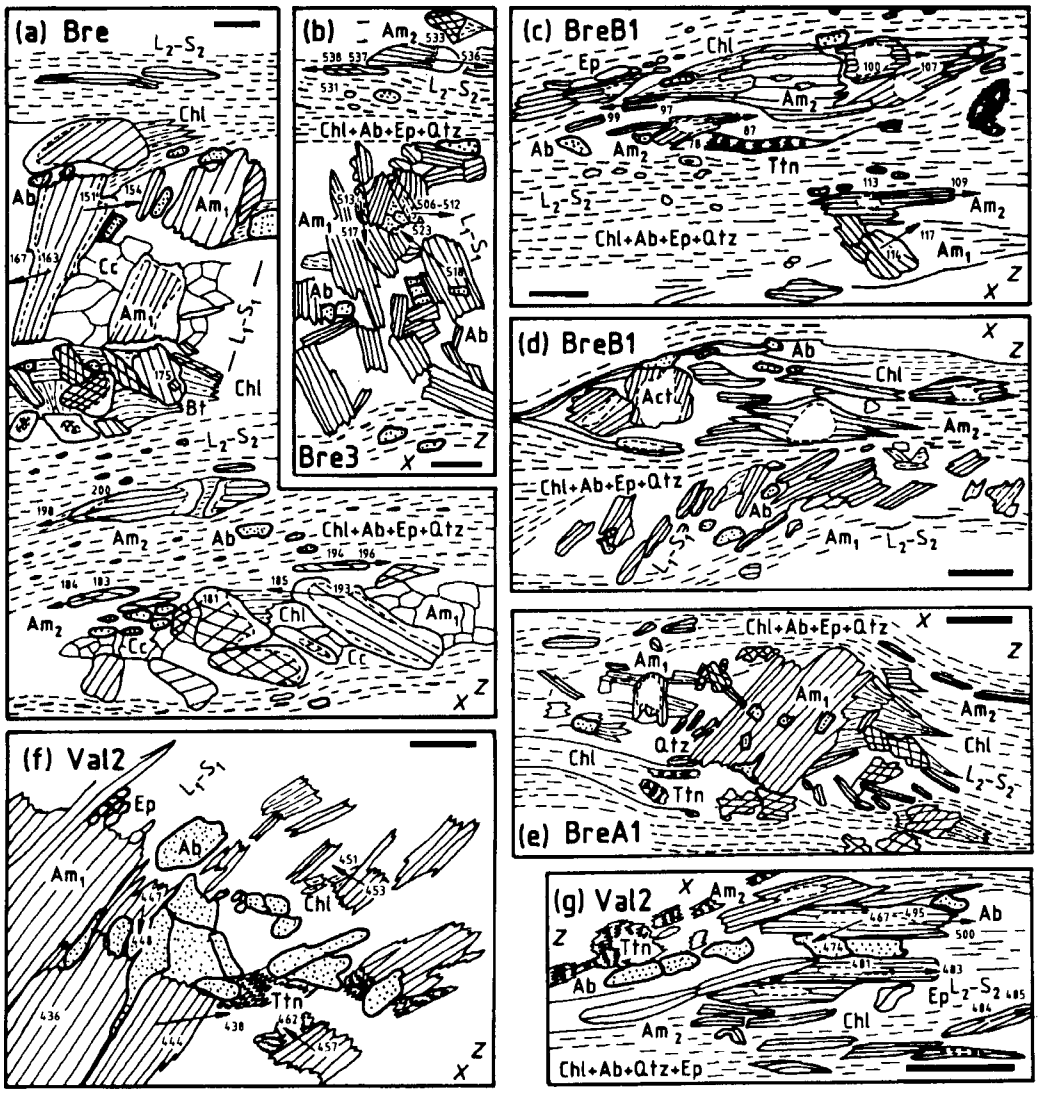

FIG. 3. (*a*)–(*g*) Microstructures in an amphibolite horizon from the Lower Schieferhülle. Scale bar is 0.5 mm. X–Z sections parallel to L_2-S_2. Act—actinolite; Am—amphibole; Ab—albite; Bt—biotite; Cc—calcite; Chl—chlorite, Ep—epidote; Qtz—quartz; Ttn—titanite. Green amphibole is hatched, actinolite is not hatched. Arrows indicate core–rim profiles of microprobe analyses (numbers) in Fig. 6.

actinolite. Domain (1) represents a preserved low-strain zone, domain (2) a high-strain zone of the partitioned foliation-forming deformation (D_2). The high strain of the progressing deformation mainly partitioned from domain (2) with S_2 into the mylonitic domain (3) with S_{myl} when temperatures decreased. The deformation persisted after the growth of late actinolite and the shearband foliation S_4 has been formed in domain (3) at conditions near to the ductile–brittle transition.

Upper Schieferhülle, (USH). Metabasites in the Upper Schieferhülle USH are former submarine ophiolitic basalts with MORB affinity (Höck, 1981; Höck and Miller, 1987; De Vecchi, 1989) and occur as thick bodies in Mesozoic calcareous and pelitic metasediments. A lithological banding of the

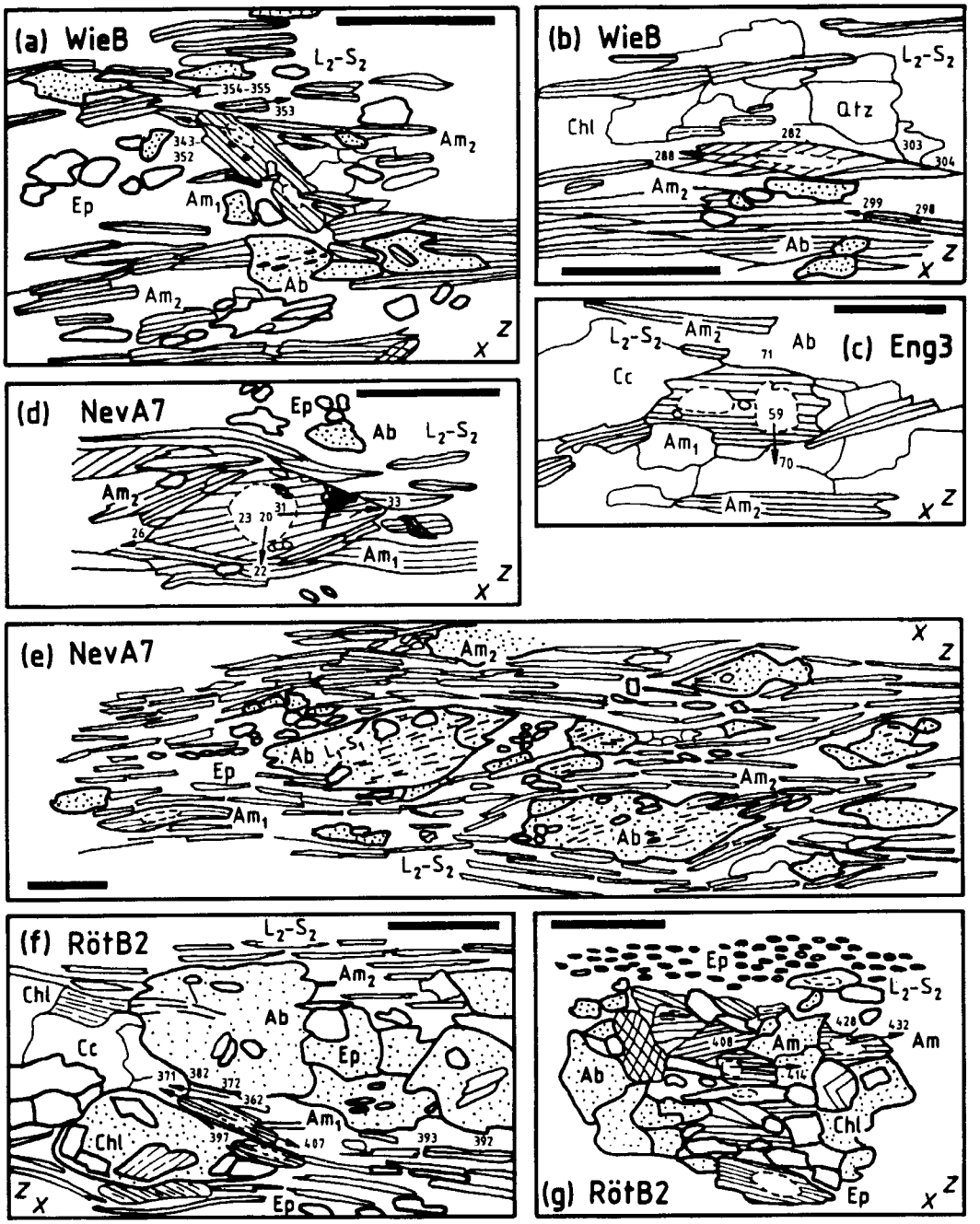

FIG. 4. (*a*)–(*g*) Microstructures in amphibolites from the Upper Schieferhülle. Scale bar is 0.5 mm. X–Z sections parallel to L_2-S_2. Act—actinolite; Am—amphibole; Ab—albite; Bt—biotite; Cc—calcite; Chl—chlorite, Ep—epidote; Qtz—quartz; Ttn—titanite. Green amphibole is hatched, actinolite is not hatched. Arrows indicate core–rim profiles of microprobe analyses (numbers) in Fig. 6.

amphibolites results from different modes of amphibole, epidote, chlorite, plagioclase and quartz in the layers. Sample locations in a large western metabasite complex in lower parts of the USH are Wieden in the Pfitschtal (WieB), the Unterbergbachtal at the Selverstone and Spear (1985) locations (MO1, MO2), the Weitenbergalm (MO3, Schulz *et al.*, 1994) and the Engbergalm (Eng3) in the upper Pfunderer Tal, and the road to the Neves lake in the Mühlbachtal (NevA7). Another metabasite complex in upper parts of the USH to the east (Raase, 1974) was sampled in the Röttal to the south of Prettau/Ahrntal (RötB2). All samples show a W–E trending lineation (= X) by preferentially oriented amphiboles and were studied in XZ sections. The mineral lineation (L_2) in metabasites and metasedimentary host rocks is parallel to and identical with fold axes of F_3 folds.

Preferentially oriented amphiboles (2) in samples MO1, MO2, MO3 and NevA7 define lineation and foliation (L_2-S_2) and surround lens- and lozenge-shaped mineral aggregates composed of epidote, chlorite, quartz and amphibole, or albite porphyroblasts with numerous inclusions of these minerals forming an L_1-S_1 fabric (Fig. 4*e*). The shapes of the mineral aggregates and microlithons appear to be the result of a non-coaxial partitioned deformation and should be distiguished from other mineral aggregates which were interpreted to testify the former presence of pseudomorphs after lawsonite (Fry, 1973; Selverstone and Spear, 1985). Long axes of large amphibole (1) porphyroblasts between the foliation planes are oriented at an acute angle to S_2 (Fig. 4*a*). In the MO1, MO2, MO3 samples, large third-generation amphiboles (3) cut across the S_2 structure defined by amphibole (2) (Schulz *et al.*, 1994). Although it is not always visible by optical methods, all three generations of amphiboles show similar prograde zonation trends from actinolite cores toward tschermakitic hornblende rims (Fig. 6*e–i*). In sample MO3, a prograde actinolite to green hornblende and a retrograde green hornblende to actinolite zonation trend (Fig. 6*f*) has been analysed (Schulz *et al.*, 1994). Zonations from actinolitic hornblende to actinolite in amphibole (2) needles of sample RötB2 (Fig. 6*i*) also refer to a retrograde stage of metamorphism. Compositions of tschermakitic hornblendes in the different samples are between $(Na+K)_A$ 0.3–0.5, Al^{VI} 0.7–0.9 and Ti 0.05–0.06 (Table 1). Plagioclase is always oligoclase (An20) in samples MO1 and MO2, and albite in samples MO3, Eng3, NevA7 and RötB2. Both oligoclase and albite occur in WieB. According to the microstructural positions it is possible to distinguish among syn-L_1-S_1 or pre-L_2-S_2 albites in the interstitial space or as porphyroblasts in microlithons, syn-L_2-S_2 albites (sometimes with thin oligoclase rims) elongated parallel to L_2-S_2 and post-L_2-S_2 porphyroblasts

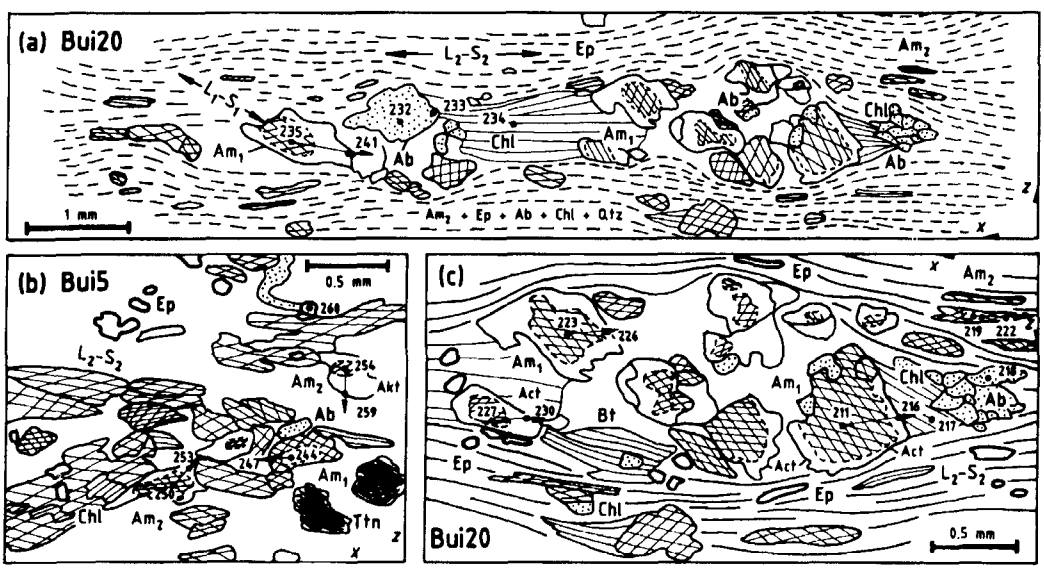

FIG. 5. (*a*)–(*c*) Microstructures in amphibolites from the Austroalpine basement to the south of the western Tauern window. X–Z sections parallel to L_2-S_2. Act—actinolite; Am—amphibole; Ab—albite; Bt—biotite; Cc—calcite; Chl—chlorite; Ep—epidote; Qtz—quartz; Ttn—titanite. Green amphibole is hatched, actinolite is not hatched. Arrows indicate core–rim profiles of microprobe analyses (numbers) in Fig. 6.

(sometimes oligoclase) which overgrew L_2-S_2. Epidotes are zoned with Fe-rich cores and Al^{3+} of 2.4 (WieB), 2.5–2.7 (MO3), 2.6 (Eng3), 2.4 (NevA7) and 2.3–2.4 (RötB2). The X_{Mg} of chlorites are constant in each sample with X_{Mg} 0.63 in WieB, 0.65 in NevA7 and 0.67 in RötB2. The assemblage (Na-Ca) amphibole–albite (oligoclase)-chlorite-epidote-quartz was stable in different microstructural sites of D_1 (preserved as L_1-S_1 in microlithons and albite porphyroblasts), D_2 with L_2-S_2 structures and post-D_2 with crystallization of post-L_2-S_2 plagioclase and amphibole (3).

Austroalpine basement (AA). The upper part of the USH is built up by alternating Mesozoic graphitic phyllites, calcschists, marbles, chlorite epidote metabasites, quartzites and serpentinites with similar Alpine linear, planar and folding structures as observed in the USH and the AA. No suitable rocks for the geothermobarometric P–T path studies were found in this 1 km thick Penninic–Austroalpine transition zone, referred to as the Lower Austroalpine Matreier zone by Tollmann (1977). Amphibolites of pre-Variscan origin (Schulz *et al.*, 1993) occur with biotite gneisses and mylonitic orthogneisses in the Austroalpine basement immediately to the south of the Matreier zone. These metabasites with a W–E striking mineral lineation by preferentially oriented amphiboles were sampled in the Kleinklausen-Tal (Hüh) and in the upper Buinlandtal (Bui5, Bui20) to the south of the Ahrntal (Fig. 1*b*). Only one generation of large zoned amphiboles (Fig. 6*k*) occur with albite and oligoclase in sample Hüh. In samples Bui5 and Bui20, the W–E striking L_2-S_2 fabric by small amphiboles (2) and fine grained epidote, chlorite, albite and quartz surrounds up to cm-long microlithons with large amphibole (1) and coarse-grained chlorite, epidote, albite and quartz (Fig. 5*a*,*c*). Small actinolite cores of amphibole (1) are mantled by magnesio-hornblende. The porphyroblasts have rims of actinolite. Similar zonation trends were analysed in amphibole (2). Maximum contents of Al^{IV} (1.75), Al^{VI} (0.7), $(Na + K)_A$ (0.65) and Ti (0.077–0.92) in sample Bui5 are slightly higher than in sample Bui20 (Fig. 6*l*, *m*, Table 1). Plagioclase is albite in samples Bui5 and Bui20; epidotes have an Al^{3+} value of 2.3 and the X_{Mg} of chlorites is 0.63. As observed in the USH samples, the assemblage (Na-Ca) amphibole–albite–chlorite–epidote–quartz persisted in microlithons and L_2-S_2 throughout the deformation.

Geothermobarometry and P–T-deformation paths

The amphibolite samples from the LSH, USH and AA units display different microstructures of a common Alpine structural evolution with formation of L_1–S_1, L_2–S_2 and post-L_2–S_2 microfabrics. Microprobe analyses were performed on characteristic microstructural sites in selected thin sections. The chemical evolution of the amphiboles in each thin section has been checked by 5–10 profiles and/or parts of profiles of 5–15 point analyses in well-defined and clearly optically zoned porphyroblasts of the L_1-S_1, L_2-S_2 and post-L_2–S_2 microstructural sites. Chlorites, epidotes and plagioclases next to the amphibole porphyroblasts were analysed at cores and rims or by profiles of 3–5 points. As it was the aim of the study to discover the general chemical evolution of the amphiboles and the related minerals during their crystal growth, the analysis of small-scale late diffusion effects on mutual grain boundaries and inclusions has been avoided. Amphibole compositions do not change when in contact with plagioclase, whatever its composition. The individual zonations and compositions of the amphiboles in a given thin section are part of an overall and systematic chemical evolution trend in Al^{VI} *vs.* $(Na + K)_A$ coordinates (Fig. 6, Table 1). Continuous core–rim zonations with amphibole compositions connecting the actinolite and green hornblende compositional fields are observed. The equivalent zonations of amphiboles (1), (2) and (3) in the different L_1-S_1, L_2-S_2 and post-L_2-S_2 microstructural positions (USH and AA samples) and in different microstructural domains (low- and high-strain zones in Bre and Val samples) signalize a continuous crystallization in the different microstructural sites of a partitioned progressive deformation. The coeval chemical evolutions of the amphiboles in Al^{VI} (pressure sensitive), $(Na + K)_A$ and Ti (temperature sensitive) with prograde actinolite to tschermakitic hornblende and retrograde magnesio-hornblende to actinolite zonation trends are similar in the studied samples. In the 100Na/(Ca + Na) *vs.* 100Al/(Si + Al) and Na_{M4} *vs.* $Na_A + K$ diagrams of Laird and Albee (1981), the amphibole compositions plot in the medium pressure field next to the low pressure field.

It is well known that the composition of the host rock with its influence on the mineral chemistry, and the compositions of the amphiboles and paragenetic minerals are determinant factors in the application of the different methods used to follow P–T variations during metamorphism (e.g. Leake, 1965; Harte and Graham, 1975; Grapes *et al.*, 1977; Thiéblemont *et al.*, 1988). The distribution of Si, Al and Na in amphibole sites depends on the physical conditions of crystallization. Si^{4+} increases, Al^{VI} and $(Na_A + Na_{M4})$ decrease when the grade of metamorphism decreases (Boyd, 1954; Bard, 1970). Na_A increases with temperature (Vittel and Fabriès, 1982) as does Ti (Raase, 1974; Laird & Albee, 1981; Colombi, 1989). Al^{VI} and Na_{M4} increase with pressure at

constant temperature (Leake, 1965; Brown, 1977). Amphibole–plagioclase assemblages exist over a wide $P-T$ range. Low-T/low- to high-P plagioclase is albite. At low pressure, plagioclase becomes Ca-rich when temperatures increases. Even at 600°C an amphibole rich in Na_A may be in equilibrium with albite (Spear, 1980; 1981).

The Holland and Richardson (1979) geothermobarometer cannot be applied to the western Tauern metabasite samples due to the negligible glaucophane

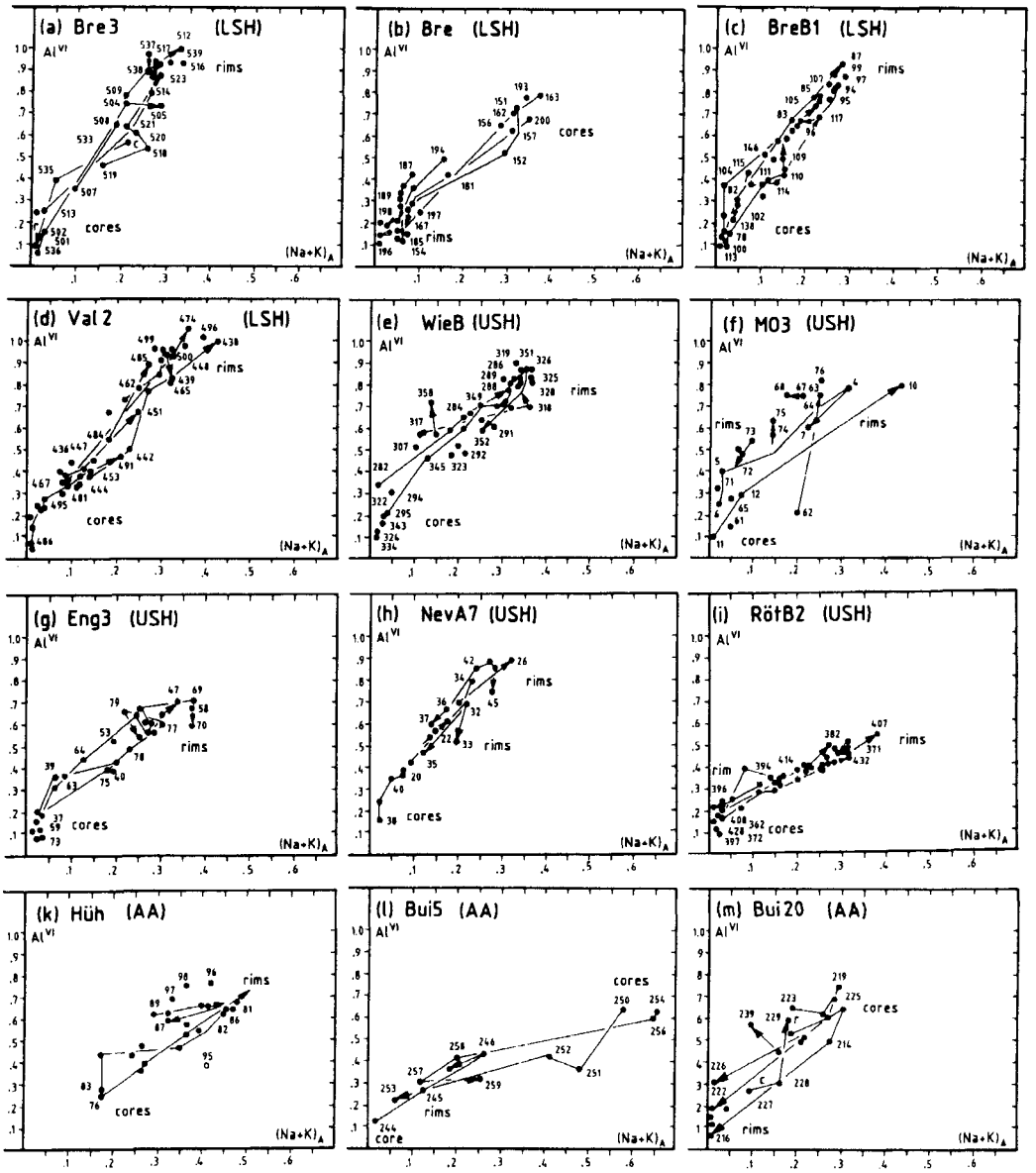

FIG. 6. (*a*)–(*m*) Mineral chemical evolution of amphiboles in samples from the Mesozoic Lower Schieferhülle (LSH), the Upper Schieferhülle (USH) and the Austroalpine basement (AA) in Al^{VI} (= relative pressure) *vs.* $(Na + K)_A$ (= relative temperature) coordinates. Numbers are microprobe analyses in Figs 3–5. Arrows indicate temporal direction of the compositional evolution according to core–rim zonation trends in the amphiboles.

activities in the analysed amphiboles. The maximum temperatures or the thermal peak of metamorphism have been estimated with the empirical Al^{IV}/Ti geothermobarometer of Colombi (1989). From magnesio-hornblendes and tschermakitic hornblendes, temperatures around 600°C at pressures of 6–7 kbar have been obtained. A more accurate interpretation of the amphiboles mineral chemistry evolution in terms of $P-T$ data is possible with the (Na-Ca) amphibole–albite–chlorite–epidote–quartz geothermobarometer in the system S-A-F-M-C-N-H_2O (Triboulet, 1992; Triboulet *et al.*, 1992). It is based on an empirical calibration which takes into account two equilibria. These equilibria involve edenite-tremolite and (pargasite-hastingsite)-tremolite end-members in the amphiboles of assemblages with chlorite, epidote, albite and quartz.

Cation formulae of amphiboles were calculated after the procedure explained in Triboulet (1992) with the site allotment proposed by Leake (1978) and with estimates of Fe^{3+} after Papike (1974) and Papike *et al.* (1974): (1) four Si in the *T*2 site; (2) the remaining Si and Al in the *T*1 site, with $Si + Al^{IV} = 4$; (3) the remaining Al, Ti, Fe^{3+}, Fe^{2+}, Mn and Mg in the *M*2 site, with sum *M*2 = 2; (4) Ca and Na in the *M*4 site, with $Ca + Na_{M4} = 2$; the remaining Na, K and then vacancy in the *A* site with sum *A* = 1. For the partition of Fe^{2+} and Mg between the *M*2 and (*M*1, *M*3) sites, it is assumed that $(Fe^{2+}/Mg)_{M2} = (Fe^{2+}/Mg)_{M1,M3} = (Fe^{2+}/Mg)_{amphibole}$.

Knowing the Si_{T1}, Al^{IV}, Al^{VI}, Fe^{3+}, Fe^{2+}, Mg, Ca, Na_{M4}, Na_A and *A* vacancy in an amphibole, and the Al^{3+} and X_{Mg} in coexisting epidote and chlorite, it is possible to calculate two values of ln K_d for this assemblage and to determine $P-T$ directly from each amphibole analysis (the calculation program and isopleths are reported in Triboulet, 1992). The calibration can be used when the amphibole composition can be defined by end-member activities occurring in the two equilibria considered, and when the plagioclase is albite with An < 10% (Triboulet, 1992). Samples with oligoclase only (MO1, MO2 from the Selverstone and Spear (1985) location, BreA1) are therefore not suitable for the application of this geothermobarometer. However, results of tentative geothermobarometric calculations from these samples do not differ significantly from the $P-T$ data obtained from samples with both albite and oligoclase (Bre3, BreB1, WieB, Hüh) and albite only. In samples with both oligoclase and albite, oligoclase (An20) is either late/post-L_2-S_2 and does not influence the $P-T$ paths or it occurs during the paths calculated with pure albite. In the latter case, temperatures are overestimated as the paths are shifted toward higher *T* when plagioclase is Ca-richer as An 10 %. No shifting in pressures has been observed (Triboulet, 1992).

Chlorites in the successive equilibria of the other samples raise a problem as these minerals appear with homogeneous compositions due to a possible re-equilibration during metamorphism. In contrast, the epidote compositions vary with the microstructural site and slight zonations are abundant. As a re-equilibration is not necessarily evident in most cases, a change of the modal ratios between some minerals involved in mass transfer reactions during metamorphism would reduce the compositional variations of the other minerals during the exchange. This would enable a stronger zoning of amphiboles in a closed chemical system. As the X_{Mg} of chlorites in samples with unzoned amphiboles have been found to be related to the X_{Mg} of the amphiboles (Thiéblemont *et al.* 1988), the X_{Mg} of chlorite have been varied with the different X_{Mg} of amphiboles for ln K_d calculations. Measured values of Al^{3+} in epidote were used. The remaining uncertainty on chlorite and epidote compositions leads to systematic error, which cannot be checked, on ln K_d for tremolite–(pargasite–hastingsite). However, the resulting uncertainty on ln K_d and on $P-T$ position is very small, as the stoichiometric coefficients for chlorite and epidote are low in the used equilibria (Triboulet 1992). Moreover, as the amphibole site allotment and Fe^{3+} estimation procedure has an influence on K_d values when the isopleths positions are calculated in $P-T$ coordinates, the choice of the amphibole structural formulae calculation is determined by the applied geothermobarometric calibration. The error in the standard-state enthalpy change calibration $\Delta(\Delta H°)$ cannot be estimated and the uncertainties in endmember activities and on thermodynamic constants are not known. Errors in *T* and *P* (50°C/500 bar, Fig. 7*a*) are based on the uncertainties in the microprobe analyses (in per cent: SiO_2 0.4; TiO_2 3.5; Al_2O_3 0.8; FeO 1.5; MnO 8; MgO 0.6; CaO 0.9; Na_2O 2.5; K_2O 8). Known and unknown uncertainties from microprobe analyses, thermodynamic parameters, activity models, Fe^{3+} calculations, do not change the relative positions of $P-T$ estimates in $P-T$ space and the principal shapes of the $P-T$ paths remain preserved.

Possible changes of chemical profiles by internal diffusion in the interior of amphiboles are difficult to assess. When zonation profiles of different porphyroblasts are compared, similar zonations are observed from different locations within porphyroblasts with different sizes and from several porphyroblast generations within a given sample. This provides no hints to possible internal diffusive changes in the amphiboles.

The geothermobarometric data from the amphiboles affords a reconstruction of $P-T$ evolution with a direct correlation to the structures of the Alpine deformation. In the LSH, prograde $P-T$ paths from

TABLE 1. Microprobe analyses from amphiboles in metabasites from the western Tauern Window (LSH, USH) and its southern Austroalpine (AA) frame. Selected from 800 analyses. Numbers of oxygens: 23. Fe^{3+} after Papike *et al.* (1974). Tr-Ed = ln K_d tremolite-edenite; (P-H)-Tr = lnK_d (pargasite-hastingsite)-tremolite

	BreB1								WieB					RötB2			
	78	82	85	87	94	145	137	138	282	317	318	351	352	429	430	399	400
SiO_2	55.60	52.05	47.19	45.13	46.64	53.97	50.94	52.63	50.28	48.21	43.44	42.95	43.11	53.06	50.07	51.17	51.11
TiO_2	0.02	0.13	0.34	0.41	0.36	0.10	0.17	0.12	0.23	0.34	0.30	0.53	0.54	0.20	0.18	0.09	0.15
Al_2O_3	0.75	5.16	11.31	13.87	11.47	3.36	6.56	4.57	7.11	9.29	13.20	14.75	14.62	3.99	6.71	5.13	5.72
FeO	10.56	11.15	12.68	13.91	12.82	9.95	11.30	10.72	14.46	15.00	17.80	17.44	17.41	12.03	13.36	13.74	13.77
MnO	0.21	0.26	0.32	0.31	0.32	0.24	0.26	0.24	0.25	0.25	0.29	0.25	0.20	0.24	0.24	0.20	0.22
MgO	17.11	15.68	12.22	10.78	12.07	16.91	14.89	16.03	13.56	11.83	9.33	8.81	8.561	15.80	13.91	14.18	13.83
CaO	12.48	12.06	11.60	11.28	11.61	12.52	11.87	12.39	11.11	11.38	11.49	11.40	11.32	11.54	11.41	10.86	10.90
Na_2O	0.16	0.62	1.32	1.67	1.38	0.41	0.76	0.50	0.97	1.72	1.97	1.69	1.65	0.90	1.31	1.22	1.28
K_2O	0.08	0.23	0.27	0.32	0.29	0.19	0.25	0.13	0.23	0.25	0.44	0.39	0.35	0.11	0.23	0.16	0.20
Total	96.97	97.34	97.25	97.68	96.96	97.65	97.00	97.33	98.20	97.68	97.66	98.21	97.76	97.87	97.42	96.75	97.18
Si	7.945	7.428	6.831	6.541	6.786	7.652	7.309	7.510	7.141	6.985	6.398	6.303	6.358	7.521	7.219	7.383	7.363
Al^{IV}	0.055	0.572	1.169	1.459	1.214	0.348	0.691	0.490	0.859	1.015	1.602	1.697	1.642	0.479	0.781	0.617	0.637
Al^{VI}	0.072	0.298	0.765	0.916	0.757	0.215	0.420	0.280	0.334	0.574	0.695	0.859	0.905	0.189	0.361	0.257	0.336
Ti	0.002	0.014	0.037	0.045	0.039	0.011	0.018	0.013	0.025	0.037	0.033	0.058	0.060	0.021	0.020	0.010	0.016
Fe^{3+}	0.086	0.325	0.283	0.394	0.287	0.142	0.306	0.212	0.831	0.438	0.748	0.550	0.464	0.467	0.424	0.614	0.492
Fe^{2+}	1.176	1.005	1.252	1.292	1.273	1.037	1.049	1.067	0.886	1.378	1.443	1.589	1.683	0.958	1.186	1.043	1.166
Mn	0.025	0.031	0.039	0.038	0.039	0.029	0.032	0.029	0.030	0.031	0.036	0.031	0.025	0.029	0.029	0.024	0.027
Mg	3.647	3.338	2.693	2.331	2.620	3.577	3.187	3.412	2.873	2.557	2.050	1.929	1.883	3.341	2.992	3.052	2.972
Ca	1.909	1.843	1.798	1.751	1.809	1.901	1.823	1.893	1.690	1.782	1.717	1.791	1.788	1.751	1.761	1.678	1.681
Na_{M4}	0.091	0.157	0.202	0.249	0.191	0.099	0.177	0.107	0.310	0.218	0.283	0.209	0.212	0.249	0.239	0.322	0.319
Na_A	0.001	0.015	0.169	0.221	0.199	0.014	0.035	0.031	0.001	0.069	0.281	0.273	0.260	0.001	0.128	0.020	0.040
K	0.015	0.042	0.050	0.059	0.054	0.034	0.046	0.024	0.042	0.046	0.083	0.073	0.066	0.020	0.042	0.029	0.037
□	1.032	0.944	0.781	0.720	0.747	0.952	0.919	0.945	1.001	0.884	0.636	0.654	0.674	0.981	0.829	0.951	0.924
X_{Mg}	0.756	0.769	0.678	0.643	0.673	0.775	0.752	0.762	0.764	0.650	0.587	0.548	0.528	0.777	0.716	0.745	0.718
$X_{Fe^{3+}}$	0.545	0.522	0.270	0.301	0.275	0.398	0.422	0.431	0.713	0.433	0.519	0.390	0.339	0.712	0.540	0.705	0.594
Tr-Ed	−8.90	−3.78	−0.10	0.51	0.10	−4.32	−2.58	−3.13	−5.87	−1.38	1.04	1.07	0.93	−6.63	−1.00	−3.31	−2.55
(P-H)-Tr	−14.4	−5.26	−0.85	0.09	−0.64	−7.18	−4.10	−5.38	−6	−2.26	0.77	0.72	0.53	−8.4	−2.38	−4.53	−4
	Act	ActH	MgH	MgH	MgH	Act	ActH	Act	MgH	MgH	TsH	TsH	TsH	Act	ActH	ActH	ActH

Table 1 (*contd.*)

	RötB2				Bui20							Bui5					
	432	433	394	395	227	219	211	223	214	239	222	244	247	254	250	259	253
SiO_2	46.69	49.51	50.46	54.60	52.61	45.69	47.35	48.96	45.27	50.61	55.35	53.31	48.57	48.71	42.16	46.56	50.21
TiO_2	0.22	0.24	0.19	0.03	0.09	0.52	0.53	0.24	0.41	0.18	0.04	0.00	0.12	0.78	0.46	0.21	0.09
Al_2O_3	9.49	6.69	6.35	2.72	4.82	11.91	9.54	9.93	10.20	7.63	2.72	2.11	6.74	12.31	11.77	8.09	4.35
FeO	15.15	13.17	14.36	11.45	13.05	13.91	13.24	12.05	14.82	12.68	10.83	15.59	19.19	21.79	21.57	18.77	17.72
MnO	0.22	0.22	0.33	0.30	0.35	0.25	0.30	0.28	0.28	0.30	0.35	0.39	0.21	0.40	0.22	0.26	0.48
MgO	12.24	13.75	13.55	15.98	14.87	11.24	12.68	13.37	11.73	13.28	16.76	13.60	10.18	6.05	6.62	10.40	11.41
CaO	11.56	11.51	10.68	11.07	12.17	11.64	11.28	11.67	11.04	10.76	12.78	11.17	10.97	10.63	10.29	10.53	11.13
Na_2O	1.64	1.23	1.60	0.89	0.81	1.40	1.39	1.36	1.68	1.43	0.30	0.61	1.40	1.78	2.06	1.69	0.84
K_2O	0.27	0.15	0.19	0.09	0.14	0.40	0.20	0.20	0.26	0.19	0.09	0.08	0.27	1.80	1.46	0.54	0.34
Total	97.48	96.47	97.71	97.13	98.91	96.96	96.51	98.06	95.69	97.06	99.22	96.86	97.65	96.25	96.61	97.05	96.57
Si	6.812	7.216	7.240	7.764	7.462	6.701	6.902	7.747	6.707	7.284	7.747	7.758	7.186	6.357	6.499	6.906	7.459
Al^{IV}	1.188	0.784	0.760	0.236	0.538	1.299	1.098	0.253	1.293	0.716	0.253	0.242	0.814	1.643	1.501	1.094	0.541
Al^{VI}	0.448	0.367	0.317	0.220	0.270	0.763	0.544	0.197	0.492	0.581	0.197	0.120	0.363	0.627	0.642	0.323	0.222
Ti	0.024	0.026	0.020	0.003	0.010	0.057	0.058	0.004	0.046	0.019	0.004	0.000	0.013	0.092	0.053	0.023	0.010
Fe^{3+}	0.543	0.368	0.640	0.356	0.274	0.259	0.466	0.102	0.673	0.316	0.102	0.420	0.450	0.332	0.399	0.776	0.410
Fe^{2+}	1.305	1.236	1.082	1.005	1.273	1.446	1.148	1.165	1.162	1.210	1.165	1.477	1.973	2.513	2.381	1.551	1.791
Mn	0.027	0.027	0.040	0.036	0.042	0.031	0.037	0.042	0.035	0.037	0.042	0.048	0.026	0.053	0.029	0.033	0.060
Mg	2.664	2.989	2.900	3.390	3.146	2.459	2.757	3.499	2.593	2.851	3.499	2.952	2.247	1.409	1.522	2.301	2.528
Ca	1.806	1.796	1.641	1.685	1.848	1.828	1.760	1.915	1.751	1.658	1.915	1.740	1.738	1.777	1.698	1.672	1.770
Na_{M4}	0.194	0.204	0.359	0.315	0.152	0.172	0.240	0.085	0.249	0.342	0.085	0.260	0.262	0.223	0.302	0.328	0.230
Na_A	0.271	0.144	0.087	0.001	0.071	0.227	0.154	0.001	0.235	0.058	0.001	0.001	0.140	0.317	0.315	0.159	0.013
K	0.050	0.028	0.035	0.016	0.025	0.075	0.037	0.016	0.049	0.035	0.016	0.015	0.051	0.358	0.287	0.102	0.064
□	0.679	0.828	0.878	1.052	0.903	0.699	0.809	0.987	0.716	0.907	0.987	0.999	0.809	0.324	0.398	0.739	0.923
X_{Mg}	0.671	0.707	0.728	0.771	0.71	0.63	0.70	0.75	0.69	0.70	0.75	0.66	0.54	0.36	0.39	0.60	0.58
$X_{Fe^{3+}}$	0.548	0.501	0.669	0.617	0.504	0.25	0.46	0.34	0.58	0.35	0.34	0.77	0.55	0.34	0.38	0.70	0.65
Tr-Ed	0.47	−0.91	−1.51	−7.42	−2.15	0.39	−0.38	−0.44	0.39	−2.02	−7.35	−7.40	−0.87	1.86	1.50	−0.26	−3.86
(P-H)-Tr	−0.40	−2.40	−2.50	−10.10	−4.06	−0.06	−1.10	−1.13	0.35	−3.14	−10.44	−9.72	−2.15	0.78	0.49	−0.68	−5.55
	MgH	MgH	MgH	Act	ActH	MgH	MgH	Act	MgH	ActH	Act	Act	MgH	TsH	TsH	MgH	ActH

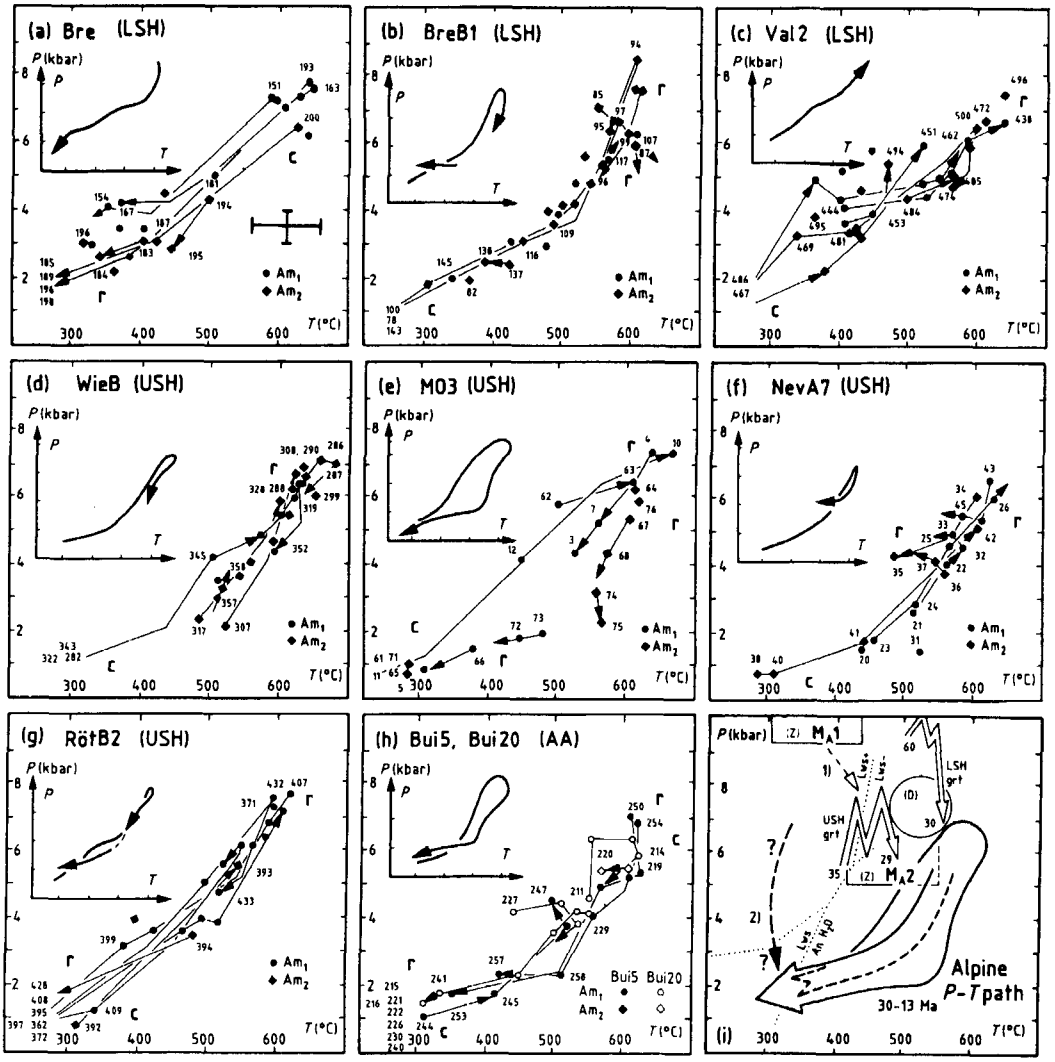

FIG. 7. (*a*)–(*h*) *P*–*T* data and *P*–*T* paths (see inset sketches) of the Alpine greenschist-amphibolite facies metamorphism in the western Tauern Window (Mesozoic Lower Schieferhülle LSH, Upper Schieferhülle USH) and its southern Austroalpine (AA) frame. Results from the application of the Triboulet (1992) geothermobarometer (see text). Arrows indicate temporal direction of the *P*–*T* paths according to core–rim zonation trends in the Am_1 and Am_2 amphiboles. Numbers are amphibole analyses in Figs 3–6. Path from Bre is equivalent to BreB1, path from Eng3 is similar to WieB and path from Hüh corresponds to Bui20/Bui5. The error bar for each *P*–*T* point is ± 50°C/ 0.5 kbar. (*i*) Alpine *P*–*T* path, summarized from (*a*)–(*h*). Cooling ages (13–30 Ma) for this *P*–*T* path are taken from Borsi *et al.* (1978), Raith *et al.* (1978), Blanckenburg *et al.* (1989), Christensen *et al.* (1994) and Zimmermann *et al.* (1994). *P*–*T* data for the Alpine blueschist facies event M_A1 and the greenschist-amphibolite facies event M_A2 are from Holland and Ray (1985), Dachs (1990) (D), Zimmermann *et al.* (1994) (Z). The *P*–*T* paths (grt) from USH and Palaeozoic LSH garnet-bearing rocks (Selverstone, 1993) with Rb-Sr ages (Christensen *et al.*, 1994) are shown for comparison. Broken arrows: (1) Previous interpretations with M_A1 and M_A2 as successive events belonging to a common *P*–*T* loop. (2) Possible relationship between an early M_A1 event, the lawsonite stability field (e. g. Spear, 1993), and an independent later greenschist-amphibolite-greenschist facies *P*–*T* loop (see text for the discussion).

lower greenschist facies conditions of 300°C/2 kbar to the amphibolite facies at 600°C/7kbar are observed. A deviation from the average prograde $P-T$ paths toward higher pressures (Fig. 7*c*) in sample Val2 is probably related to Fe^{3+}-poor exsolutions in actinolitic cores. The retrograde evolution passes a segment at 400°C/3–4 kbar and ends at LT/LP greenschist facies conditions (Fig. 7*a–c*). Prograde and retrograde parts of the $P-T$ evolution were both recorded by amphiboles in domains (1) and (2); however, it is clear from the fine-grained actinolite–chlorite–epidote–quartz assemblages in S_2 and S_{myl} that high strain of deformation has been concentrated on the foliation planes. Formation of S_{myl} and S_4 occurred when the $P-T$ path passed lower greenschist facies conditions between 350 and 300°C.

Maximum $P-T$ conditions of 600°C/6 kbar in the USH were reached by relatively temperature-dominated $P-T$ paths which started at 300°C/1–2 kbar and show a pressure increase at 450°C in some samples (Fig. 7*d–f*). At higher temperatures, the prograde paths are outside the lawsonite stability field. Post-P_{max} paths, especially from sample MO3, are characterized by marked decompression at higher temperatures as the compression paths, and with first increasing then decreasing temperatures. When complete retrograde paths have been recorded (samples MO3, RötB2), they show significant cooling at 2–3 kbar (Fig. 7*e, g*).

Maximum conditions in the amphibolites Bui5 and Bui20 from the lowest part of the Austroalpine basement are 600°C/6.5 kbar. The prograde $P-T$ evolution in this unit is also first dominated by temperature then by pressure with a pressure increase at 450°C/3 kbar. The post-P_{max} paths show decompression/cooling to 500°C/3 kbar, then dominant cooling to final LT-LP conditions (Fig. 7*h*).

Conclusions and implications to tectonic models

Although differences in details exist, the syndeformational $P-T$ paths from AA, USH and the Mesozoic LSH have similar general shapes, first temperature-dominated, then clockwise with a final cooling at low pressures. The paths started in the lower greenschist facies passed the epidote–amphibolite facies at P_{max} then T_{max} and finished at greenschist facies conditions again (Fig. 7*i*). Maximum temperatures for the Alpine greenschist–amphibolite facies event in all three units are 600°C from the Colombi (1989) and Triboulet (1992) geothermobarometers. These temperatures are 50–100°C higher as has been previously estimated from other rocks and with other geothermobarometric calibrations (Hoernes and Friedrichsen, 1974; De Vecchi and Baggio, 1982; Selverstone and Spear, 1985; Frank *et al.*, 1987; Dachs, 1990). At least a part of these differences could be caused by the empirical calibrations of the (Na-Ca) amphibole geothermobarometer. Results from garnet–biotite thermometry in garnet muscovite schists of the AA are 550–580°C (Schulz, 1990, and unpublished data) and in fair agreement with the data from the amphibolites. If temperatures are slightly overestimated by the geothermobarometers of Colombi (1989) and Triboulet (1992) , the principal shapes of the $P-T$ paths will not change dramatically, as pressures are equivalent to the previous results (Fig. 7*i*). As is evident from the geothermobarometric calculations, the mineral chemistry and the mineral assemblages, the samples belong to the same metamorphic zone which cuts across the tectonostratigraphic units. Complete $P-T$ paths are observed from single samples and locations, and the $P-T$ estimates do not represent a metamorphic field gradient from a random pattern of $P-T$ data from scattered samples.

Minimum ages of the metamorphism are given by Rb-Sr, K-Ar and Ar-Ar mineral data (Borsi *et al.*, 1978; Raith *et al.*, 1978; Blanckenburg *et al.*, 1989; Christensen *et al.*, 1994; Zimmermann *et al.*, 1994). Following the concept of closure temperatures and interpreting biotite Rb-Sr ages to date the cooling below 320°C, the minimum age of the final retrograde stage of the $P-T$ paths is 13–15 Ma (Blanckenburg *et al.*, 1989). Low-silica micas yield Ar-Ar data which indicate cooling at 27 Ma in the central Tauern Window (Zimmermann *et al.*, 1994). According to the Rb-Sr data from garnets in the LSH and USH, the thermal climax in the western Tauern Window may have been around 30 Ma and P_{max} in the Palaeozoic LSH at 60 Ma (Selverstone, 1993; Christensen *et al.*, 1994). In the absence of fossil data from the Mesozoic host rocks of the amphibolites, or of further radiometric data, it is impossible to constrain the age when burial began.

It is evident from the syndeformational $P-T$ paths and the chemical evolution of the amphiboles that the greenschist–amphibolite facies event is similar in the AA, USH and the Mesozoic part of the LSH, and represents an independent metamorphism along a complete $P-T$ loop. Furthermore, even if minimum uncertainties of $\pm$ 50°C/$\pm$ 0.5 kbar on the geothermobarometric calculations are considered, there is no hint that the prograde paths passed high-pressure/low-temperature conditions in the studied units (Fig. 7*i*). The prograde $P-T$ evolution was dominated by an increase of temperatures with a moderate increase of pressures and the $P-T$ ratios are situated in the $P-T$ range of a 'continental orogenic belt' metamorphism (Spear, 1993). It is possible that the short anticlockwise portions of some

prograde paths have been related to an early ephemeral temperature-dominated heat flow regime.

According to the $P-T$ data from the amphibolites, a high-pressure/low-temperature event in the Tauern Window should have predated the greenschist–amphibolite–greenschist facies $P-T$ loop. Pressure may have decreased from high-pressure/low-temperature conditions previous to the prograde greenschist–amphibolite facies evolution. Lozenge-shaped mineral aggregates have been interpreted as pseudomorphs after lawsonite of a high-pressure/low-temperature event (e.g. Selverstone and Spear, 1985). Alternatively, lawsonite may have crystallized at low-pressure/low-temperature conditions at the beginning of the $P-T$ path (Fig. 7*i*). This appears possible, as lawsonite can be stable at LP-LT conditions. Additionally the actual pressures for the growth of early actinolite in the amphibolites may have been slightly underestimated by the Triboulet (1992) calibration due to the low activity of pargasite–hastingsite end-members in actinolites.

This observation of a complete greenschist–amphibolite–greenschist facies $P-T$ loop contrasts the interpretations of Holland and Ray (1985) and Zimmermann *et al.* (1994) for the central Tauern Window with that of Selverstone and Spear (1985) for the western Tauern Window. These authors assigned the glaucophane–lawsonite or blueschist facies and the greenschist–amphibolite facies metamorphic stages in the USH to a common $P-T$ loop (Fig. 7*i*). The $P-T$ paths confirm the results of De Vecchi and Baggio (1982) who found no evidence of a blueschist facies event in the USH metabasites of the western Tauern Window. However, the geothermobarometric data from garnet-bearing rocks in the Palaeozoic LSH of the western Tauern Window (Selverstone *et al.*, 1984) and the data from the Eclogite zone in the central Tauern Window (Fig. 7*i*) indicate quite different $P-T$ evolutions in basal and upper parts of the nappe pile.

This complete middle- to late-Alpine greenschist–amphibolite facies $P-T$ loop is coeval with a polyphase Alpine deformation. The boundary between the Mesozoic Matreier zone/Upper Schieferhülle and the pre-Variscan Austroalpine basement is clearly a marked lithological boundary in the Eastern Alps. However, the continuous structural transition across the boundary, the similar late-Alpine radiometric ages on both sides and the common metamorphic evolution obvious from similar $P-T$-deformation paths, suggest that Mesozoic units and the Austroalpine basement rocks were imbricated and welded prior to the thermal and baric peaks of the greenschist–amphibolite facies event. Accordingly, crustal burial with a stacking (D_1) of AA, USH and LSH nappes and with a movement of the nappes parallel to the lineation, then isoclinal folding F_2 (D_2), could be associated with the prograde paths. The uplift after P_{max} was then accompanied by subsequent transpression tectonics with folding F_3 (D_3) around the W-E trending lineation. At a late stage of the uplift, the top-to-W directed movements of low-angle normal faulting occur along S_{myl} and S_4 planes with a W–E directed lineation. In this manner, the prograde as well as the retrograde $P-T$ evolution are associated with L_1-S_1, L_2-S_2 then F_3, S_{myl} and S_4 structures of a polyphase progressive deformation with a constantly W–E oriented extension axis of strain.

There arise some consequences for geodynamic models of the Alpine evolution. It is clear from the significant differences in maximum pressures between the Eclogite zone on the one hand and the AA, USH and Mesozoic LSH on the other hand, that these units have not been adjacent throughout their metamorphic histories. Furthermore, the glaucophane–lawsonite or blueschist event in the EZ, LSH and USH was not related to the greenschist–amphibolite facies $P-T$-loop and appears to be an earlier event. After individual burial histories, the high-pressure and medium-pressure units should have been brought together during the uplift of the high-pressure rocks, as has been outlined by Spear (1993, p. 744–745). Accordingly, Frank *et al.* (1987) explained the temporal and spatial relationships by envisaging two subduction zones — an early-Alpine subduction to the north with an early high-pressure metamorphism, and a later middle- to late-Alpine second subduction to the south with the greenschist–amphibolite facies metamorphism. However, the moderate $P-T$ ratios in the studied AA, USH and Mesozoic LSH favour a continental collisional type of metamorphism rather than subduction for the second event. Similar Alpine two-stage successive subduction-uplift then collision-uplift processes have been recognized from metamorphic rocks of the Betic Cordilleras (Puga *et al.*, 1989).

Acknowledgements

Most of the microprobe analyses were facilitated by F. S. Spear during a research stay of B. S. at the Rensselaer Polytechnic Institute, Troy, New York, USA. Further analytical work has been performed with M. Bohn at IFREMER Brest and M. Fialin, Laboratoire de Pétrologie Minéralogique at Paris, France. M. Oehlke, München, and C. Wölfel, Erlangen, accompanied the sampling in the Hohe Tauern. Constructive remarks by an anonymous reviewer improved the manuscript. The study was financed by a grant from the Deutsche Forschungsgemeinschaft (Schu 676/2-4) to B.S. and funds of the Centre National de la Recherche Scientifique of France.

References

Bard, J.P. (1970) Compositions of hornblendes during the Hercynian progressive metamorphism of the Aracene metamorphic belt (SW Spain). *Contrib. Mineral. Petrol.*, **28**, 117–34.

Behrmann, J.H. (1990) Zur Kinematik der Kontinentkollision in den Ostalpen. *Geotektonische Forschungen*, **76**, 1–180.

Blankenburg, F. von, Villa, I.M., Baur, H., Morteani, G. and Steiger, R.H. (1989) Time calibration of a PT-path from the western Tauern Window, Eastern Alps: the problem of closure temperatures. *Contrib. Mineral. Petrol.*, **101**, 1–11.

Borsi, S., Del Moro, A., Sassi, F.P., Zanferrari, A. and Zirpoli, G. (1978) New geopetrologic and radiometric data on the Alpine history of the Austridic continental margin south of the Tauern Window. *Mem. Ist. Geol. Min. Univ. Padova,* **32**, 1–17.

Boyd, F.R. (1954) Amphiboles. *Carnegie Inst. Washington Year.*, **53**, 108–11; Washington.

Brown, E.H. (1977) The crossite content of Ca-amphibole as a guide to pressure of metamorphism. *J. Petrol.*, **18**, 53–72.

Christensen, J.N., Selverstone, J., Rosenfeld, J.L. and DePaolo, D.J. (1994) Correlation by Rb-Sr geochronology of garnet growth histories from different structural levels within the Tauern Window, Eastern Alps. *Contrib. Mineral. Petrol.*, **118**, 1–12.

Colombi, A. (1989) Métamorphisme et géochimie des roches mafiques des Alpes ouest-centrales (géoprofil Viège–Domodossola–Locarno). *Mémoires de Géologie*, **4**, 1–216; Lausanne.

Dachs, E. (1990) Geothermobarometry in metasediments of the southern Grossvenediger area (Tauern Window, Austria). *J. Metam. Geol.*, **8**, 217–30.

Dachs, E., Frasl, G. and Hoinkes, G. (1991) Mineralogisch-petrologische Exkursion ins Penninikum des Tauernfensters und in das Ötztalkristallin. *Euro. J. Mineral.*, **3**, 79–110.

De Vecchi, G. (1989) Metaophiolitic suite in the south-western Tauern Window (Italian sector). *Mem. Sci. Geol.*, **41**, 51–9 (Padova).

De Vecchi, G. and Baggio, P. (1982) The Pennine zone of the Vizze region in the western Tauern Window (Italian Eastern Alps). *Boll. Soc. Geol. Ital.*, **101**, 89–116.

De Vecchi, G. and Mezzacasa, G. (1986) The Pennine basement and cover units in the Mesule Group (south-western Tauern Window). *Mem. Sci. Geol.*, **38**, 365–92 (Padova).

Frank, W., Höck, V. and Miller, C. (1987) Metamorphic and tectonic history of the Central Tauern Window. In *Geodynamics of the Eastern Alps* (H.W. Flügel and P. Faupl, eds.), 34–54. Franz Deuticke Verlag, Vienna.

Frisch, W. (1976) Ein Modell zur alpidischen Evolution und Orogenese des Tauernfensters. *Geol. Rundsch.*, **65**, 375–93.

Frisch, W. (1980) Post-Hercynian formations of the western Tauern Window: Sedimentological features, depositional environment, and age. *Mitt. Österr. Geol. Ges.*, **71/72**, 49–63.

Frisch, W. (1984): Metamorphic history and geochemistry of a low-grade amphibolite in the Kaserer formation (marginal Bündner Schiefer of the western Tauern Window, the Eastern Alps). *Schweiz. Mineral. Petrogr. Mitt.*, **64**, 193–214.

Fry, N. (1973) Lawsonite pseudomorphed in Tauern greenschist. *Mineral. Mag.*, **39**, 121–22.

Grapes, R.H., Hashimoto, S. and Miyashita, S. (1977) Amphiboles of a metagabbro-amphibolite sequence, Hiddaka metamorphic belt, Hokkaido. *J. Petrol.*, **18**, 285–319.

Grundmann, G. and Morteani, G. (1985) The young uplift and thermal history of the central Eastern Alps (Austria/Italy), evidence from apatite fission track ages. *Jahrb. Geol. B.-A.*, **128**, 197–216.

Hammerschmidt, K. (1981) Isotopengeologische Untersuchungen am Augengneis vom Typ Campo Tures bei Rain in Taufers, Südtirol. *Mem. Ist. Geol. Min. Univ. Padova*, **34**, 273–300.

Harte, B. and Graham, C.M. (1975) The graphical analysis of greenschist to amphibolite facies mineral assemblages in metabasites. *J. Petrol.*, **16**, 347–70.

Höck, V. (1969) Zur Geologie des Gebietes zwischen Tuxer Joch und Olperer (Zillertal, Tirol). *Jahrb. Geol. B.-A.*, **112**, 163–95.

Höck, V. (1980) Distribution maps of minerals of the Alpine metamorphism in the Penninic Tauern Window, Austria. *Mitt. Österr. Geol. Ges.*, **71/72**, 119–27.

Höck, V. (1981) Ophiolitic and non-ophiolitic metabasic rocks in the Penninic zone of the Hohe Tauern (Eastern Alps, Austria). *Ofioliti*, **6**, 1–23.

Höck, V. and Miller, Ch. (1987) Mesozoic ophiolitic sequences and non-ophiolitic metabasites in the Hohe Tauern. In *Geodynamics of the Eastern Alps* (W.H. Flügel and P. Faupl, eds), 16–33. Franz Deuticke Verlag, Vienna.

Höck, V. and Hoschek, G. (1980) Metamorphism of calcareous metasediments in the Hohe Tauern, Austria. *Mitt. Österr. Geol. Ges.*, **71/72**, 99–118.

Hoernes, S. and Friedrichsen, H. (1974) Oxygen isotope studies on metamorphic rocks of the western Tauern Window area (Austria). *Schweiz. Mineral. Petrogr. Mitt.*, **54**, 769–88.

Hofmann, K.H., Kleinschrodt, R., Lippert, R., Mager, D. and Stöckhert, B. (1983) Geologische Karte des Altkristallins südlich des Tauernfensters zwischen Pfunderer Tal und Tauferer Tal (Südtirol). *Der Schlern*, **57**, 572–90, 1 Kt.; Bozen (Athesia Verlag).

Holland, T.J.B. (1979) High water activities in the generation of high pressure kyanite eclogites in the

Tauern Window, Austria. *J. Geology*, **87**, 1–17.

Holland, T.J.B. and Ray, N.J. (1985) Glaucophane and pyroxene breakdown reactions in the Pennine units of the Eastern Alps. *J. Metam. Geol.*, **3**, 417–38.

Holland, T.J.B. and Richardson, S.W. (1979) Amphibole zonation in metabasites as a guide to the evolution of metamorphic conditions. *Contrib. Mineral. Petrol.*, **70**, 143–48.

Kleinschrodt, R. (1987) Quarzkorngefügeanalyse im Altkristallin südlich des westlichen Tauernfensters (Südtirol/Italien). *Erlanger geol. Abh.*, **114**, 1–82.

Laird, J. and Albee, A.L. (1981) Pressure, temperature, and time indicators in mafic schists: their application to reconstructing the polymetamorphic history of Vermont. *Am. J. Sci.*, **281**, 127–75.

Lammerer, B. (1986) Das Autochthon im westlichen Tauernfenster. *Jahrb. Geol. B.-A.*, **9**, 51–67.

Lammerer, B. (1988) Thrust-regime and transpression regime tectonics in the western Tauern Window (Eastern Alps). *Geol. Rundsch.*, **77**, 143–56.

Lammerer, B. and Morteani, G. (1990) Exkursionsführer Schlegeis und Pfitscher Joch, Zillertaler Alpen, MINPET 90, Neukirchen am Großvenediger. *Mitt. Österr. Mineral. Ges.*, **135**, 185–97.

Lammerer, B., Schmidt, K. and Stadler, R. (1981) Zur Stratigraphie und Genese der penninischen Gesteine des südwestlichen Tauernfensters. *N. Jb. Geol. Paläont. Mh.*, 11, 678–96.

Leake, B.E. (1965) The relationship between tetrahedral aluminium and the maximum possible octahedral aluminium in natural calciferous and subcalciferous amphiboles. *Amer. Mineral.*, **50**, 843–54.

Leake, B.E. (1978) Nomenclature of amphiboles. *Mineral. Mag.*, **42**, 533–63.

Miller, Ch. (1977) Chemismus und phasenpetrologische Untersuchungen der Gesteine der Eklogitzone des Tauernfensters. *Tschermaks Mineral. Petrogr. Mitt.*, **24**, 221–77.

Miller, Ch., Satir, M. and Frank, W. (1980) High-pressure metamorphism in the Tauern Window. *Mitt. Österr. Geol. Ges.*, **71/72**, 89–97.

Morteani, G. (1971) Gliederung und Metamorphose der Serien zwischen Stilluptal und Schlegeistal. *Verh. Geol. B.-A.*, 287–314.

Morteani, G. (1974) Petrology of the Tauern Window, Austrian Alps. *Fortschr. Mineral.*, **52**, 195–220.

Nollau, G. (1969) Kleintektonische Strukturen am Südrand des Tauernfensters und ihre Einbeziehung in großtektonische Konzepte. *Geol. Rundsch.*, **58**, 755–88.

Oehlke, M., Weger, M. and Lammerer, B. (1993) The "Hochfeiler Duplex" — imbrication tectonics in the SW Tauern Window. *Abh. Geol. B.-A.*, **49**, 107–24.

Papike, J.J. (1974) On the chemistry of clinoamphiboles. *EOS Trans. Geophys. Union*, **55**, 469.

Papike, J.J., Cameron, K.C. and Baldwin, K. (1974) Amphiboles and pyroxenes: characterization of other than quadrilateral components and estimate of ferric iron from microprobe data. *Geol. Soc. Abstr. Progr. 6*, 1053.

Puga, E., Diaz de Federico, A., Fediukova, E., Bondi, M. and Morten, L. (1989) Petrology, geochemistry and metamorphic evolution of the ophiolitic eclogites and related rocks from the Sierra Nevada (Betic Cordilleras, Southeastern Spain). *Schweiz. Mineral. Petrogr. Mitt.*, **69**, 435–55.

Raase, P. (1974) Al and Ti contents of hornblende, indicators of pressure and temperature of regional metamorphism. *Contrib. Mineral. Petrol.*, **45**, 231–236.

Raith, M., Hörmann, P.K. and Abraham, K. (1977) Petrology and metamorphic evolution of the Penninic ophiolites in the western Tauern Window (Austria). *Schweiz. Mineral. Petrogr. Mitt.*, **57**, 187–232.

Raith, M., Mehrens, C. and Thöle, W. (1980) Gliederung, tektonischer Bau und metamorphe Entwicklung der penninischen Serien im südlichen Venediger-Gebiet, Osttirol. *Jahrb. Geol. B.-A.*, **123**, 1–37.

Raith, M., Raase, P., Kreuzer, H. and Müller, P. (1978) The age of the Alpidic metamorphism in the Western Tauern Window, Austrian Alps, according to radiometric dating. In *Alps, Apennines, Hellenides* (H. Closs, D.H. Roeder and K. Schmidt, eds), 140–8.

Sander, B. (1912) Über einige Gesteinsgruppen des Tauernwestendes. *Jahrb. k. u. k. geol. Reichsanst.*, **70** (3/4), 273–96.

Sander, B. (1921) Geologische Studien am Westende der Hohen Tauern. Zweiter Bericht. *Jahrb. Geol. St.-A.*, **70**, 273–96.

Schön, C. and Lammerer, B. (1993) Strainanalyse an grobklastischen Metasedimenten des westlichen Tauernfensters. *Abh. Geol. B.-A.*, **49**, 97–106.

Schulz, B. (1990) Tectonic significance of an early-Alpine *P–T*-deformation path from Austroalpine micaschists to the south of the Tauern Window, Eastern Alps. *Schweiz. Mineral. Petrogr. Mitt.*, **70**, 403–17.

Schulz, B. (1994) Geologische Karte 1 : 50 000 des Altkristallins östlich des Tauferer Tals (Südtirol). *Erlanger geol. Abh.*, **124**, 1–28.

Schulz, B., Nollau, G., Heinisch, H. and Godizart, G. (1993) Austro-Alpine basement complex to the south of the Tauern Window. In *Pre-Mesozoic Geology in the Alps* (J.F. von Raumer, J.F. and F. Neubauer, eds), 493–512, Heidelberg (Springer Verlag).

Schulz, B., Oehlke, M., Audren, C. and Triboulet, C. (1994) Évolution pression-temperature-temps-déformation d'âge Alpin des amphibolites du SW de la fenêtre des Tauern (Alpes orientales). *C. R. Acad. Sci. Paris*, **318/II**, 1483–8.

Selverstone, J. (1988) Evidence for east–west crustal extension in the Eastern Alps: implications for the

unroofing history of the Tauern Window. *Tectonics*, **7**, 87–105.

Selverstone, J. (1993) Micro- to macroscale interactions between deformational and metamorphic processes, Tauern Window, Eastern Alps. *Schweiz. Mineral. Petrogr. Mitt.*, **73**, 229–39.

Selverstone, J. and Spear, F.S. (1985) Metamorphic *P–T* paths from pelitic schists and greenstones from the south-west Tauern Window, Eastern Alps. *J. Metamorphic Geol.*, **3**, 439–65.

Selverstone, J., Spear, F.S., Franz, G. and Morteani, G. (1984) High-pressure metamorphism in the SW Tauern Window, Austria: *P–T* paths from hornblende-kyanite-staurolite schists. *J. Petrol.*, **25**, 501–31.

Senarclens-Grancy, W. (1972) Geologische Karte der westlichen Deferegger Alpen 1 : 25000. *Geol. B.-A. Österreich (ed.)*, Wien.

Spear, F.S. (1980) NaSi–CaAl exchange equilibrium between plagioclase and amphibole: an empirical model. *Contrib. Mineral. Petrol.*, **80**, 140–6.

Spear, F.S. (1981) An experimental study of hornblende stability and compositional variability in amphibolite. *Amer. J. Sci.*, **281**, 697–734.

Spear, F.S. (1993) Metamorphic Phase Equilibria and Pressure-Temperature-Time Paths. *Mineralogical Society of America Monograph Series*, **1**, 799 pp.

Spear, F.S. and Franz, G. (1986) *P–T* evolution of metasediments from the Eclogite Zone, south-central Tauern Window, Austria. *Lithos*, **19**, 219–34.

Spear, F.S. and Selverstone, J. (1983) Quantitative *P–T* paths from zoned minerals: theory and tectonic applications. *Contrib. Mineral. Petrol.*, **83**, 348–57.

Stöckhert, B. (1984) K-Ar determinations on muscovites and phengites and the minimum age of the Old Alpine deformation in the Austridic basement south of the Tauern Window (Ahrn valley, Southern Tyrol, Eastern Alps). *Neues Jahrb. Mineral., Abh.*, **150**, 103–20.

Thiéblemont, D., Triboulet, C. and Godard, G. (1988) Mineralogy, petrology and *P–T*-t path of Ca-Na amphibole assemblages, Saint-Martin-des-Noyers formation, Vendée, France. *J. Metam. Geol.*, **6**, 697–715.

Thiele, O. (1970) Zur Stratigraphie und Tektonik der Schieferhülle der westlichen Hohen Tauern. *Verh. Geol. B.-A.*, 230–44.

Tollmann, A. (1977) *Geologie von Österreich*, Band 1. Die Zentralalpen. 766 pp., Wien (Deuticke Verlag).

Triboulet, C. (1992) The (Na-Ca)amphibole-albite-chlorite-epidote-quartz geothermobarometer in the system S–A–F–M–C–N–H_2O. 1. An empirical calibration. *J. Metam. Geol.*, **10**, 545–56.

Triboulet, C. and Audren, C. (1988) Controls on *P–T*-t deformation path from amphibole zonation during progressive metamorphism of basic rocks (estuary of the River Vilaine, South Brittany, France). *J. Metam. Geol.*, **6**, 117–33.

Triboulet, C., Thiéblemont, D. and Audren, C. (1992) The (Na-Ca)amphibole-albite-chlorite-epidote-quartz geothermobarometer in the system S–A–F–M–C–N–H_2O. 2. Applications to metabasic rocks in different metamorphic settings. *J. Metam. Geol.*, **10**, 557–66.

Vittel, G. and Fabriès, J. (1982) Characterization de l'évolution polymétamorphique du Hoggar central (Sahara) basée sur l'analyse cristallochimique d'amphiboles calciques. *Bull. Minéral.*, **105**, 110–24.

Zimmermann, R., Hammerschmidt, K. and Franz, G. (1994) Eocene high pressure metamorphism in the Penninic units of the Tauern Window (Eastern Alps): evidence from ^{40}Ar-^{39}Ar dating and petrological investigations. *Contrib. Mineral. Petrol.*, **117**, 175–86.

[*Manuscript received 31 October 1994: revised 16 December 1994*]